Marine Chemistry 219 (2020) 103751

Contents lists available at ScienceDirect

Marine Chemistry

journal homepage: www.elsevier.com/locate/marchem

Sources of particulate Ni and Cu in the water column of the northern South China Sea: Evidence from elemental and isotope ratios in aerosols and sinking particles

Shotaro Takano[a,*], Wen-Hsuan Liao[b], Hung-An Tian[b], Kuo-Fang Huang[c], Tung-Yuan Ho[b], Yoshiki Sohrin[a]

[a] Institute for Chemical Research, Kyoto University, Uji, Kyoto 611-0011, Japan
[b] Research Center for Environmental Changes, Academia Sinica, Taipei, Taiwan
[c] Institute of Earth Sciences, Academia Sinica, Taipei, Taiwan

A B S T R A C T

We present isotope ratios of Ni (δ^{60}Ni) and Cu (δ^{65}Cu) in sinking particles, aerosols, and seawater collected from the northern South China Sea to identify sources and transformation processes of the two metals. In aerosols, δ^{60}Ni values are in the range +0.05‰ to +0.56‰, and δ^{65}Cu values are in the range −0.33‰ to +0.83‰. The isotope ratios are different from those of lithogenic materials, indicating that the aerosols are anthropogenic in origin. In sinking particles collected at depths of 2000 and 3500 m, δ^{60}Ni values are in the range +0.01‰ to +0.54‰ at 2000 m and −0.18‰ to +0.54‰ at 3500 m, and the values exhibit similar temporal variation pattern between 2000 and 3500 m. Based on the significant correlation between δ^{60}Ni and the ratio of P/Ni or organic-C/Ni, we hypothesize that the main sources of Ni in the sinking particles originate from both resuspended marine sediments off southwest Taiwan, and biogenic organic particles. The δ^{60}Ni in biogenic particles is estimated to be +0.6‰ to +1.0‰, which is 0.3–0.7‰ lighter than that of dissolved Ni in seawater. The isotope ratios of Cu in sinking particles are fairly constant (+0.13‰ to +0.36‰), and the range is between those of marine sediments and labile fractions of marine particles. Thus, Cu in sinking particles is likely to be from marine sediments and biogenic organic particles. Compared with Ni, the correlation between Cu and P or organic-C is weaker, suggesting that the Cu/P and Cu/organic-C ratios are not constant in organic matter or there are additional sources of particulate Cu, such as Fe-Mn oxides and anthropogenic aerosols.

1. Introduction

Trace metals, such as Ni and Cu, can be essential nutrients and/or toxins for marine phytoplankton and influence primary productivity in the ocean (e.g., Morel and Price, 2003). Due to the important roles of trace metals in material cycling, studies during the past 40 years have revealed vertical distribution patterns of the concentrations of many dissolved trace metals (e.g., Boyle et al., 1977, 1981; Bruland, 1980). The international GEOTRACES program was further established to investigate the large spatial scale distribution patterns of trace metals and isotopes in the global ocean. However, trace metal isotope studies are still limited in the global ocean. Isotopic compositions are powerful tools to identify sources and transformation processes of materials in geochemical and environmental studies, owing to their specific isotopic fractionation through chemical, physical, and biological processes, such as redox reactions, biological uptake, adsorption, and phase transitions (Teng et al., 2017). Isotope ratios of Cu and Ni are generally expressed in δ^{60}Ni and δ^{65}Cu:

$$\delta^{60}Ni = [(^{60}Ni/^{58}Ni)_{Sample}/(^{60}Ni/^{58}Ni)_{NIST\ SRM\ 986} - 1] \times 1000$$

$$\delta^{65}Cu = [(^{65}Cu/^{63}Cu)_{Sample}/(^{65}Cu/^{63}Cu)_{NIST\ SRM\ 976} - 1] \times 1000$$

In seawater, reported dissolved δ^{60}Ni ranges from +1.3‰ to +1.7‰ (Cameron and Vance, 2014; Takano et al., 2017; Wang et al., 2019), which is significantly higher than the mean value of +0.15 ± 0.12‰ (mean ± 2SD [two standard deviations]) observed in lithogenic materials (Elliott and Steele, 2017). For Cu, δ^{65}Cu in seawater ranges from +0.4‰ to +0.9‰ (Baconnais et al., 2019; Little et al., 2018; Takano et al., 2014; Thompson and Ellwood, 2014; Vance et al., 2008), and the range is also higher than the mean value of +0.07‰ ± 0.10‰ in lithogenic materials (Moynier et al., 2017). The global means in river water, which is believed to be the main source of dissolved Ni and Cu to the ocean, are +0.80‰ for δ^{60}Ni (Cameron and Vance, 2014) and +0.68‰ for δ^{65}Cu (Vance et al., 2008). The dominant sink for dissolved Ni and Cu in the ocean is considered to be Fe–Mn oxides (Little et al., 2014; Vance et al., 2016). Based on the analysis of hydrogenetic Fe–Mn crusts, the isotope ratios associated with this sink range from +0.8‰ to +2.5‰ for δ^{60}Ni (Gall et al., 2013; Gueguen et al., 2016) and from +0.05‰ to +0.60‰ for δ^{65}Cu (Little et al., 2014). Euxinic and organic-rich sediments are suggested to

* Corresponding author.
E-mail address: takano.shotaro.3r@kyoto-u.ac.jp (S. Takano).

https://doi.org/10.1016/j.marchem.2020.103751

Available online 08 January 2020

be additional sinks of Ni and Cu, with different isotope ratios from those of Fe–Mn oxides (Ciscato et al., 2018; Little et al., 2017). However, the oceanic budgets for dissolved Ni and Cu are elementally and isotopically imbalanced, suggesting missing sources or sinks of Ni and Cu (Cameron and Vance, 2014; Ciscato et al., 2018; Little et al., 2014; Vance et al., 2016).

Sinking particles play important roles in biogeochemical cycling of trace metals in the ocean by transporting materials from the surface to the deep ocean and provide direct information on the oceanic sink of trace metals in the ocean. Sinking particles are mainly composed of lithogenic, biogenic, and authigenic particles. Lithogenic particles are supplied to the ocean mainly via atmospheric deposition (Duce et al., 1991) and resuspension of marine sediments (Ho et al., 2011). Biogenic particles are produced in the surface ocean; they concentrate trace metals through biological uptake (Twining and Baines, 2013; Twining et al., 2014) and/or adsorption onto their surface from seawater (Balistrieri et al., 1981; John and Conway, 2014; Weber et al., 2018), and transport the trace metals to the deep ocean. Authigenic Fe–Mn oxides are suggested to be responsible for the adsorption of trace metals (Sherrell and Boyle, 1992). Anthropogenic particles are another source of trace metals in oceanic regions influenced by intense human activity (Liao et al., 2017). In addition to the various sources, the isotopic compositions of sinking particles not only possess the original signals of the sources but may also reflect the transformation processes of particles during transport from the surface to deep water.

The northern South China Sea (NSCS) is an ideal oceanic region to investigate the relative contributions of natural and anthropogenic materials to the ocean, as the region receives a large amount of lithogenic and anthropogenic materials through the atmosphere. Both lithogenic and anthropogenic aerosols from East Asia are transported to the NSCS surface water by the northeast monsoon in winter and spring. Previous studies have demonstrated that anthropogenic aerosols are major sources of trace metals in suspended particles in surface water of the NSCS (Ho et al., 2007, 2010). Pacyna and Pacyna (2001) estimate that anthropogenic emissions account for 76% and 48% of global atmospheric emissions for Ni and Cu, respectively. Nickel is known as one of the most abundant metals in crude oil (Barwise, 1990). Fossil fuel combustion accounts for 90% of the anthropogenic emissions of Ni to the atmosphere (Pacyna and Pacyna, 2001). Although there are a small number of analyses, isotope ratios of Ni have been reported for some materials associated with anthropogenic sources. The δ^{60}Ni in crude oil and coal is reported to be $+0.54 \pm 0.29$‰ (Ventura et al., 2015) and $+0.47$‰ (Gueguen et al., 2013), respectively. For Cu, major anthropogenic sources are suggested to be emissions from smelting processes, vehicular traffic, and fossil fuel combustion (Ho et al., 2006; Hulskotte et al., 2007; Pacyna and Pacyna, 2001; Suvarapu and Baek, 2017). A wide range of δ^{65}Cu ($+0.0$ to $+0.6$‰) is found in aerosols collected in large cities in Europe and South America, suggesting various Cu sources (Dong et al., 2017; Gonzalez et al., 2016; Souto-Oliveira et al., 2018, 2019).

To the best of our knowledge, no systematic studies of Ni and Cu isotopes in marine sinking particles have been reported, although several recent studies have revealed dissolved Ni and Cu isotopic compositions in seawater (Cameron and Vance, 2014; Takano et al., 2014, 2017; Thompson and Ellwood, 2014; Vance et al., 2008; Wang et al., 2019). In this study, we propose a new pretreatment procedure to precisely analyze isotopic ratios for Ni and Cu in particulate samples. We then determined Ni and Cu isotope ratios in aerosols and sinking particles collected in the NSCS to investigate their major sources, to quantify the relative contributions of the sources, and to study the transformation processes of the particulate Ni and Cu in the water column.

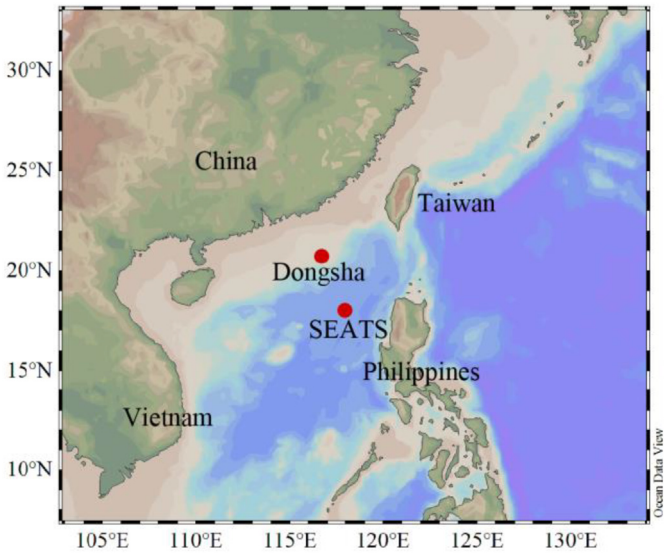

Fig. 1. Location of the South East Asian Time-series Study (SEATS; 18.0°N 116.0°E) station and Dongsha Atoll (20.7°N 116.7°E).

2. Methods

2.1. Sampling

Seawater and sinking particle samples were collected at the South East Asian Time-series Study (SEATS) station located at 18.0°N and 116.0°E in the NSCS, with a bottom depth of 3783 m (Fig. 1). Aerosol samples were collected at an onshore station on the Dongsha Atoll, which is located at 20.7°N and 116.7°E at a distance of 300 km from the SEATS station. The NSCS is influenced by two well-defined seasonal monsoons: a strong northeastern monsoon in winter and a weak southwestern monsoon in summer. Owing to these monsoon systems, seasonal primary production at the SEATS station is highest in winter and lowest in summer. Seawater samples were collected using acid-cleaned Teflon-coated Go-Flo bottles (General Oceanics) on 21 October 2006. The samples were filtered through 0.22 μm acid-cleaned polycap cartridge filters (Whatman) and subsequently transferred to acid-washed 1 L polyethylene bottles. All samples were acidified to pH 1.8 with ultrapure concentrated HCl (Seastar).

In terms of sinking particle collection, time-series moored sediment traps were deployed at depths of 2000 and 3500 m on two occasions. The first deployment lasted from 15 April 2014 to 16 October 2014, and the second from 21 November 2014 to 4 March 2015. French time-series sediment traps with a cone area of 1.00 m^2 (Technicap Pièges à Particules Séquentiels, models 5/2) were used for collecting sinking particles. The trap body and baffle material were made of reinforced polyester and phenolic composite, respectively. The cups for trapped samples were made of polypropylene and were acid-washed before use. The trap cups were filled with trap solution, which was prepared in an acid-washed polypropylene bottle by adding 800 g of Merck guarantee reagent grade NaCl to 20 L of subsurface seawater collected near the trap deployment location (Ho et al., 2011; Wen et al., 2006; Yang et al., 2012). The collection interval was 8 days for each cup. The total amounts of trace metals in sinking particles collected in the trap cups were at least two orders of magnitude greater than those in the trap solution. Thus, contamination from the trap solution was negligible. After retrieving the traps, the sample cups were detached, sealed, and stored in a cold room at 4 °C onboard the research vessel until further processing onshore.

Aerosol samples were collected using a low-volume dichotomous air sampler (Thermo Andersen SA-241). Pre-weighed polytetrafluoroethylene (PTFE) membrane filters (37 mm diameter, 1 μm pore

Table 1
Procedure for NOBIAS PA1 chelating extraction for particulate samples.

NOBIAS Chelate PA1W closed column				
Process	Solution	Volume (mL)	Flow rate (mL/min)	Flow direction
Cleaning	1 M HNO_3	20	10	Backward
Conditioning	0.03 M CH_3COOH-CH_3COONH_4	50	10	Forward
Sample loading	Sample	2–50	5	Forward
Removing lithogenic elements	2 M NH_4F	25	5	Forward
Removing NH_4F	DW	50	60	Forward
Removing NH_4F	DW	25	60	Backward
Elution	1 M HNO_3	20	4	Backward

Poly-Prep open column		
Process	Solution	Volume (mL)
Cleaning	1 M HNO_3	5
Conditioning	DW	5
Conditioning	0.03 M CH_3COOH-CH_3COONH_4	5
Sample loading	Sample	1–50
Removing lithogenic elements	2 M NH_4F	5
Removing NH_4F	DW	50
Elution	1 M HNO_3	10

size) were used as substrates. The sampler was operated at a flow rate of 16.7 L/min and collected both PM 2.5 (particle matter with an aerodynamic diameter of < 2.5 μm) and PM 2.5–10 (particle matter with a diameter from 2.5 to 10 μm) on a daily basis. The sampling period was from January to December 2011.

2.2. Elemental concentrations in sinking particles and aerosols

Prior to analysis, one-eighth of each sinking particle sample was obtained from the trap cup. The sample was filtered through a 0.2 μm polycarbonate (PC) membrane (Whatman) and further divided into three fractions; two for trace metal analysis and one for biogenic silica analysis. Each fraction was carefully weighed before subsequent analysis. For aerosol samples, the PTFE membrane with aerosol particles was first divided into two pieces; one for trace metal analysis and one for archiving. The samples were completely digested with a 5 mL mixture solution of concentrated HNO_3 and HF in Teflon vials at 120 °C for 12 h on a hot plate in a laminar flow bench in a clean laboratory. The digested solution was evaporated to dryness on the hot plate. Subsequently, the dried samples were further digested with a 5 mL mixture solution of concentrated HNO_3 and HCl. Then, the digested solution was again evaporated to dryness. The dried samples were then re-dissolved in 1 mL of concentrated HNO_3 and again evaporated to dryness. The dried aerosol samples were re-dissolved in 10 mL of 0.5 M HNO_3 and the dried sinking particle samples were re-dissolved in 8 mL of 0.5 M HNO_3 + 0.01 M HF. Reference materials, HISS-1 (marine sediment; National Research Council Canada) and BCR-414 (river plankton; European Commission) were digested in the same way as sinking particles. The elemental concentrations in each sample were analyzed using a sector field high resolution ICPMS (Thermo Fisher Scientific, Element XR) equipped with an Apex HF (Elemental Scientific). The details of the precision, accuracy, and detection limits of the method are described in previous studies (Ho et al., 2007; Liao et al., 2017).

2.3. Elemental concentrations and isotope ratios of Ni and Cu in seawater

Isotope ratios of Ni and Cu in seawater were determined using the previously developed method (Takano et al., 2017). The double spike of ^{61}Ni–^{62}Ni was added to seawater samples with a spike-to-sample ratio of 1–2 to correct for mass fractionation that occurs in column chemistry and MC-ICPMS measurements. First, Ni and Cu were collected on the NOBIAS Chelate PA1 resin (Hitachi High-Technologies) at pH 4.8. The column was cleaned with a flow of NH_4NO_3 solution (pH 4.8) followed by ultrapure water to remove matrices such as sulfate. Collected Ni and Cu were eluted with 1 M HNO_3. Pre-concentrated Ni and Cu were further purified by anion exchange with AG MP-1M resin. After sample loading into the anion exchange column, 0.4 mL of 10 M HCl was passed to elute Ni. Then, 0.7 mL of 10 M HCl was passed to remove Ti. Next, 5 mL of 4 M HCl was passed to elute Cu.

Isotope ratios of Ni and Cu were measured using a NEPTUNE Plus MC-ICPMS under a high-resolution mode for Ni and a low-resolution mode for Cu. Instrumental mass biases were corrected using a double spike technique for Ni isotopes and using an external correction technique with Ga doping for Cu isotopes. The concentration of Ni was determined with an isotope dilution method at the same time as the isotopic measurement. The concentration of Cu was measured by intensity comparison of the ^{63}Cu signal with that for bracketing standards during the MC-ICPMS measurement.

2.4. Isotope ratios of Ni, Cu, and Zn in sinking particles and aerosols

After digestion, double spikes of ^{61}Ni–^{62}Ni and ^{64}Zn–^{67}Zn were added to sinking particle and aerosol samples with a spike to sample ratio of 1–2 for both Ni and Zn. Sinking particle and aerosol samples contain large amounts of lithogenic elements, such as Al, Ti, Mn, and Fe. These metals cause interferences with isotopic measurements using MC-ICPMS, such as $^{27}Al^{37}Cl$ on ^{64}Zn, $^{47}Ti^{16}O$ on ^{63}Cu, $^{55}Mn^{16}O$ on ^{71}Ga, and ^{58}Fe on ^{58}Ni. To eliminate these elements, we developed an improved method based on NOBIAS PA1 chelate extraction (Takano et al., 2017). The procedure is shown in Table 1.

We used either of two types of NOBIAS PA1 chelate resin columns: a NOBIAS Chelate PA1W closed column (i.e., that used for seawater analysis) or a Poly-Prep open column (Bio-Rad) loaded with ~360 mg of the NOBIAS PA1 chelate resin. Solutions were passed through this column by gravity. After cleaning with 1 M HNO_3, the resin was conditioned with an acetate buffer. Then, a sample that had been dissolved in 0.5 M HNO_3 / 0.01 M HF was adjusted to pH 4.7–5.2 and passed through the column to collect metals on the resin. In this step, significant amounts of Al, Fe, Mn, and It were collected on the resin together with Ni, Cu, and Zn. To eliminate Al, Fe, Mn, and Ti, a 2 M NH_4F solution adjusted to pH 5 with an acetate buffer was eluted. The NH_4F solution was prepared by mixing ultrapure HF and NH_3 solutions. To rinse the NH_4F solution, ultrapure water was passed through the

column. Finally, 1 M HNO_3 was passed to elute Ni, Cu, and Zn. The subsequent AG MP-1M anion exchange was performed in the same way as that for seawater samples. Isotope ratios of Ni and Cu were measured using a NEPTUNE Plus MC-ICPMS under a high-resolution mode for Ni and Zn and under a medium resolution mode for Cu. Instrumental mass biases were corrected using a double spike technique for Ni and Zn isotopes and using an external correction technique with Ga or Zn doping for Cu isotopes.

3. Results

3.1. Method validation for isotopic analysis of Ni, Cu, and Zn in particulate samples

To remove major elements in lithogenic particles, we modified the NOBIAS Chelate PA1 procedure (Takano et al., 2017). The major modification is that NH_4F solution is passed through the NOBIAS Chelate PA1 column after sample loading. To evaluate the removal efficiency of the elements, a sample dissolving 10 mg of HISS-1 (i.e., marine sediment reference material) was processed using a closed column with or without NH_4F solution. When the NH_4F solution is not used, the eluate contains 2600 ± 300 ng of Al, 6500 ± 300 ng of Ti, 510 ± 30 ng of Mn, and 14,000 ± 800 ng of Fe (mean ± SD, n = 4, Fig. S1). When the NH_4F solution is used, these elements are effectively removed and the eluate contain 260 ± 130 ng of Al, 33 ± 5 ng of Ti, 0.47 ± 0.05 ng of Mn, and 37 ± 17 ng of Fe (mean ± SD, n = 6, Fig. S1). Compared with the certified concentrations (https://www.nrc-cnrc.gc.ca/eng/solutions/advisory/crm/certificates/hiss_1.html), > 99.5% of Al, Ti, Mn, and Fe are removed, and Ni, Cu, and Zn are quantitatively recovered from HISS-1 by the NOBIAS PA1 chelate extraction using NH_4F solution. Ions of Al^{3+}, Ti^{4+}, Fe^{3+}, and Mn^{2+} are hard acids that have a high affinity to fluoride ions, which is categorized as a hard base. Therefore, these metals form fluoride-complexes and are eluted with NH_4F solution.

The accuracy and precision of the new method were evaluated by analyzing reference materials of marine sediment HISS-1 and river plankton BCR-414. One hundred mg of BCR-414 and 250 mg of HISS-1 were digested. After doping the double spikes, both reference materials were divided into five portions and analyzed by the new method. The results are shown in Table 2. The concentrations of Ni, Cu, and Zn are consistent with the certified values for both HISS-1 and BCR-414. Although the isotope ratios of Ni, Cu, and Zn have not been reported for HISS-1, our results are similar to literature values for marine sediments; +0.02‰ to +0.04‰ for δ^{60}Ni (Gueguen et al., 2013), +0.04‰ to +0.32‰ for δ^{65}Cu (Little et al., 2017), and +0.17‰ to +0.79‰ for δ^{66}Zn (Maréchal et al., 2000). Our δ^{66}Zn in BCR-414 is +0.31 ± 0.03‰ (mean ± 2SD, n = 10), which is slightly lower than the reported value of 0.42‰ (Maréchal et al., 2000). Isotope ratios of Ni and Cu for BCR-414 have not been reported elsewhere and future comparisons are required.

3.2. Dissolved Ni and Cu concentrations and their isotope ratios in seawater

Concentrations and isotope ratios of Ni and Cu in seawater collected at the SEATS station are shown in Table S1. The concentrations of Ni and Cu are 5.2 nmol/kg and 3.2 nmol/kg, respectively, at a depth of 400 m, and gradually increased with depth to 9.6 nmol/kg and 5.6 nmol/kg at 3500 m. The profiles of Ni and Cu concentrations are similar to those in the Pacific Ocean (Boyle et al., 1977, 1981; Bruland, 1980; Sclater et al., 1976; Takano et al., 2014). The SEATS station isotope ratios for Ni are nearly constant at 1.4‰. In previous studies, δ^{60}Ni values are in the range of +1.3‰ to +1.4‰ in the ocean, other than for oligotrophic surface waters in the subtropical South Pacific, which has δ^{60}Ni of 1.7‰ (Cameron and Vance, 2014; Takano et al., 2017; Wang et al., 2019). For Cu, the isotope ratios are 0.5‰ at a depth of 400 m, and +0.6‰ to +0.7‰ at deeper depths. The profile is similar to previously reported profiles in the North Pacific (Takano et al., 2014).

3.3. Concentrations and isotope ratios in aerosols

The isotope ratios of Ni and Cu and the concentrations of Ni, Cu, and Ti in two size fractions of aerosols are shown in Fig. 2, Tables S2 and S3. The Ni concentrations are 0.008 ± 0.006 nmol/m^3 (mean ± SD, n = 38) for PM 2.5–10 and 0.05 ± 0.03 nmol/m^3 for PM 2.5. To determine a contribution of non-lithogenic material, Ni/Ti and Cu/Ti ratios are also shown in Fig. 2. The ratios of Ni/Ti are 0.03 ± 0.02 mol/mol for PM 2.5–10 and 0.6 ± 0.3 mol/mol for PM

Table 2
Analysis of reference materials HISS-1 and BCR-414.

	Number	Type of NOBIAS Chelate PA1 column	δ^{65}Cu [b]		[Cu] ppm	δ^{60}Ni		[Ni] ppm	δ^{66}Zn		[Zn] ppm
			Mean	2SE[a]		Mean	2SE		Mean	2SE	
HISS-1[c]	1	closed	0.06	0.05	2.06	0.07	0.05	2.32	0.18	0.04	4.48
	2	closed	0.05	0.05	2.04	0.08	0.05	2.32	0.22	0.01	4.36
	3	closed	0.06	0.06	2.05	0.00	0.06	2.34	0.22	0.02	4.32
	4	closed	0.04	0.05	2.05	0.04	0.04	2.26	0.18	0.02	4.31
	5	closed	0.06	0.05	1.97	0.04	0.04	2.26	0.21	0.02	4.34
	Mean		0.05		2.03	0.05		2.30	0.20		4.36
	2SD		0.02		0.07	0.06		0.08	0.04		0.14
BCR-414[d]	6	closed	−0.23	0.03	31.0	0.08	0.04	19.8	0.31	0.06	113
	7	closed	−0.25	0.03	31.4	0.08	0.04	19.8	0.32	0.06	113
	8	closed	−0.27	0.03	31.4	0.11	0.03	19.8	0.29	0.06	113
	9	closed	−0.27	0.03	32.2	0.10	0.03	19.8	0.30	0.06	113
	10	closed	−0.23	0.03	31.2	0.09	0.04	19.8	0.30	0.06	113
	11	open	−0.27	0.02	29.0	0.17	0.05	19.6	0.29	0.03	110
	12	open	−0.29	0.02	29.8	0.13	0.05	19.6	0.34	0.03	110
	13	open	−0.27	0.03	30.4	0.09	0.05	19.6	0.31	0.02	110
	14	open	−0.31	0.03	30.1	0.15	0.05	19.6	0.33	0.03	110
	15	open	−0.29	0.03	30.5	0.10	0.05	19.6	0.32	0.02	110
	Mean		−0.27		30.7	0.11		19.7	0.31		111
	2SD		0.05		2	0.06		0.2	0.03		3

[a] Standard errors in multicollector inductively coupled plasma mass spectrometry (MC-ICPMS) measurements.
[b] Instrumental mass bias of Cu isotopes were corrected with Zn-doping for #1–10 and Ga-doping for #11 − #15.
[c] Certified value for HISS-1 is 2.37 ± 0.37 ppm for [Cu], 2.20 ± 0.29 ppm for [Ni], and 4.90 ± 0.79 ppm for [Zn].
[d] Certified value for BCR-414 is 29.5 ± 1.3 ppm for [Cu], 18.8 ± 0.8 ppm for [Ni], and 112 ± 3 ppm for [Zn].

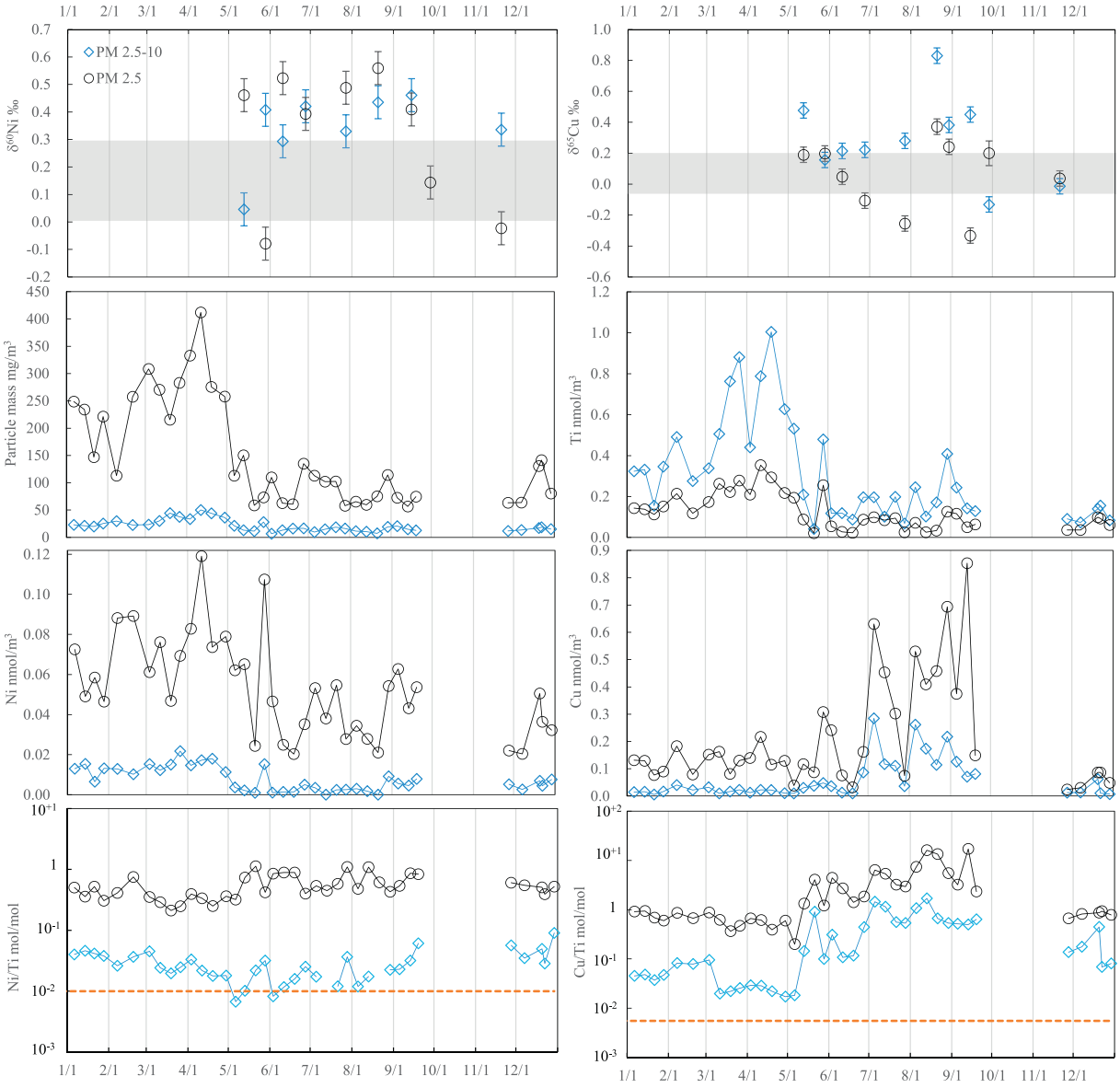

Fig. 2. Temporal variations in particle mass, metal concentrations, elemental ratios, and isotope ratios in ambient particulate matter (PM) 2.5 (circles) and PM 2.5–10 (diamonds) at Dongsha Atoll. Horizontal axis is the date in 2011. Dotted lines indicate the Ni/Ti and Cu/Ti ratios in the upper continental crust (Chester and Jickells, 2012). Gray bands indicate the mean ± 1SD (one standard deviation) for δ^{60}Ni (0.15 ± 0.12‰) and δ^{65}Cu (0.07 ± 0.10‰) in lithogenic materials (Elliott and Steele, 2017; Moynier et al., 2017). Error bars for the isotope ratios represent either 2SD of replicate analyses of BCR-414, or internal 2SE in multi-collector inductively coupled plasma mass spectrometry (MC-ICPMS) measurement when this is the larger of the of the two errors.

2.5, which are 3 times and 60 times higher than the Ni/Ti ratio of 0.01 mol/mol in the upper continental crust, respectively (Chester and Jickells, 2012). The Cu concentrations are 0.06 ± 0.07 nmol/m^3 (mean ± SD, n = 38) for PM 2.5–10 and 0.2 ± 0.2 nmol/m^3 for PM 2.5. The ratios of Cu/Ti are 0.3 ± 0.4 mol/mol for PM 2.5–10 and 3 ± 4 mol/mol for PM 2.5, which are 50 times and 500 times higher than the Cu/Ti ratio of 0.006 mol/mol in the upper continental crust, respectively (Chester and Jickells, 2012). The concentrations of Ni and Ti are higher in January–April than in May–December, while the Cu concentrations are higher in June–August. Two typhoons occurred near the sampling site at the end of May and end of August. At those times, concentrations of Ni, Cu, and Ti increased, especially for coarse aerosols (Fig. 2 and Table S2). The isotope ratios of Ni are from +0.05‰ to +0.46‰ for PM 2.5–10 and from −0.08‰ to +0.56‰ for PM 2.5. The isotope ratios of Cu are −0.13‰ to +0.83‰ for PM 2.5–10, and −0.33‰ to +0.37‰ for PM 2.5. The δ^{65}Cu values are higher in PM 2.5 than in PM 2.5–10, except for the winter aerosols.

3.4. Elemental fluxes (Ni, Cu, Ti, and P) and isotope ratios (Ni and Cu) in sinking particles

Fluxes of Ni, Cu, Ti, and P in sinking particles at depths of 2000 and 3500 m are shown in Fig. 3 and Table S4. Phosphorus mainly originates from biogenic particles, and the fluxes are higher at 2000 m than at 3500 m, particularly during winter, due to the decomposition of organic matter. Titanium is used as a tracer of lithogenic particles (Ohnemus and Lam, 2015). The fluxes of Ni, Cu, Ti, and P concordantly decrease from 23 April to 24 October and increase from 28 November to the end of February. This pattern is also observed for fluxes of biogenic silica, organic carbon (OC), and metals in sinking particles in the NSCS (Ho et al., 2011; Ran et al., 2015). Temporal changes in Ni and Cu fluxes follow that of Ti fluxes (Fig. 3 and Table S4). To determine the sources of Ni and Cu in sinking particles, the ratios against Ti are also shown in Fig. 3. The Ni/Ti ratios of 0.027 ± 0.006 mol/mol at a depth of 2000 m and 0.022 ± 0.003 mol/mol at a depth of 3500 m are

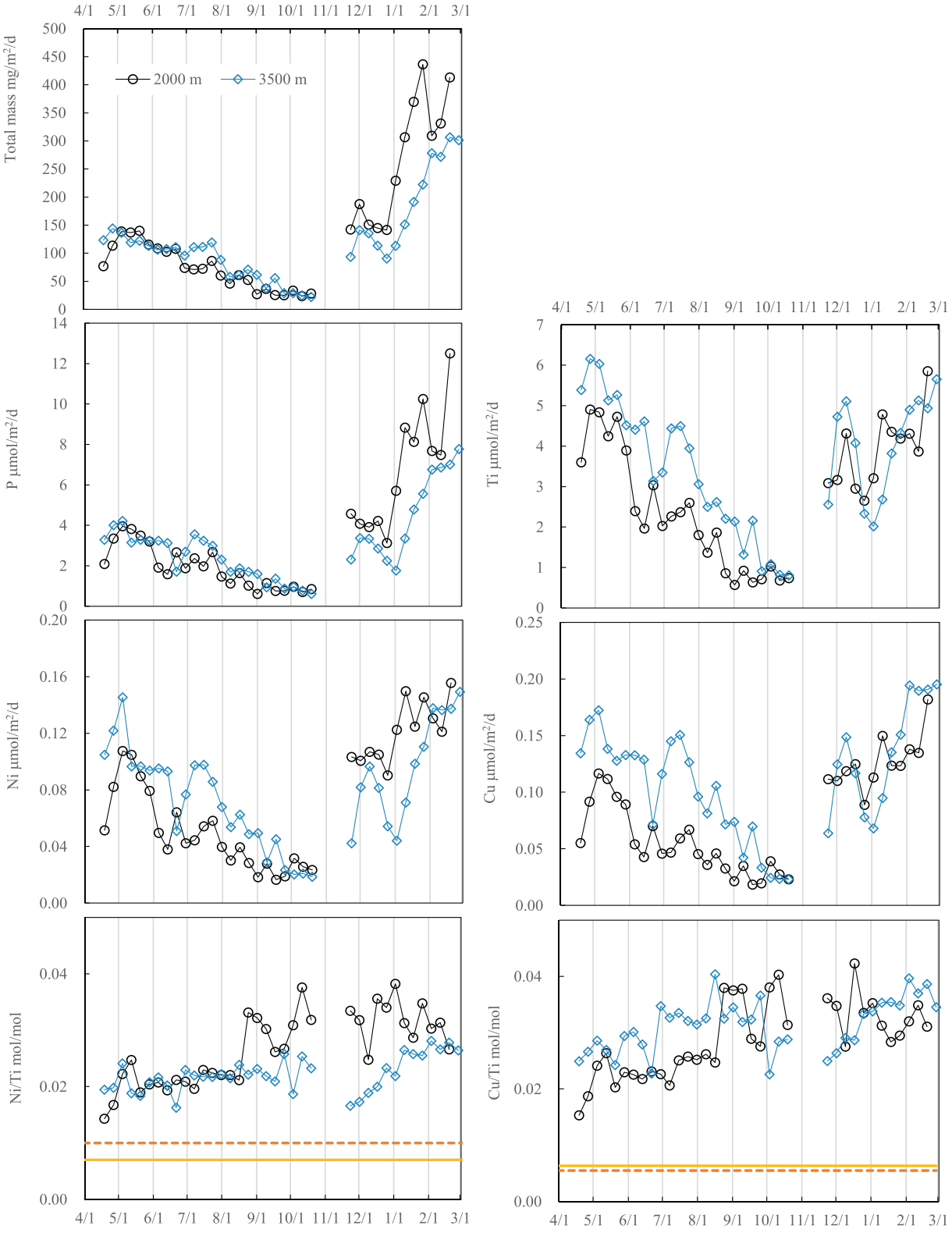

Fig. 3. Temporal variations in particle mass fluxes, elemental fluxes, and elemental ratios for sinking particles at depths of 2000 m (circles) and 3500 m (diamonds). The horizontal axis is the date from April 2014 to March 2015. Orange dotted lines indicate the Ni/Ti and Cu/Ti ratios in marine sediments off southwestern Taiwan (Chen and Kandasamy, 2008). Yellow lines indicate the Ni/Ti and Cu/Ti ratios in the upper continental crust (Chester and Jickells, 2012). (For interpretation of the references to colour in this figure legend, the reader is referred to the web version of this article.)

higher than those in marine sediments off southwestern Taiwan (0.0071 ± 0.0004 mol/mol, mean ± 1SD; Chen and Kandasamy, 2008). In particular, from the end of August to the middle of February, Ni/Ti ratios at a depth of 2000 m are significantly higher (0.032 ± 0.004 mol/mol). The Cu/Ti ratios of 0.029 ± 0.007 mol/mol at a depth of 2000 m and 0.031 ± 0.005 mol/mol at a depth of 3500 m are also higher than that in marine sediments (0.0060 ± 0.0010 mol/mol, mean ± 1SD; Chen and Kandasamy,

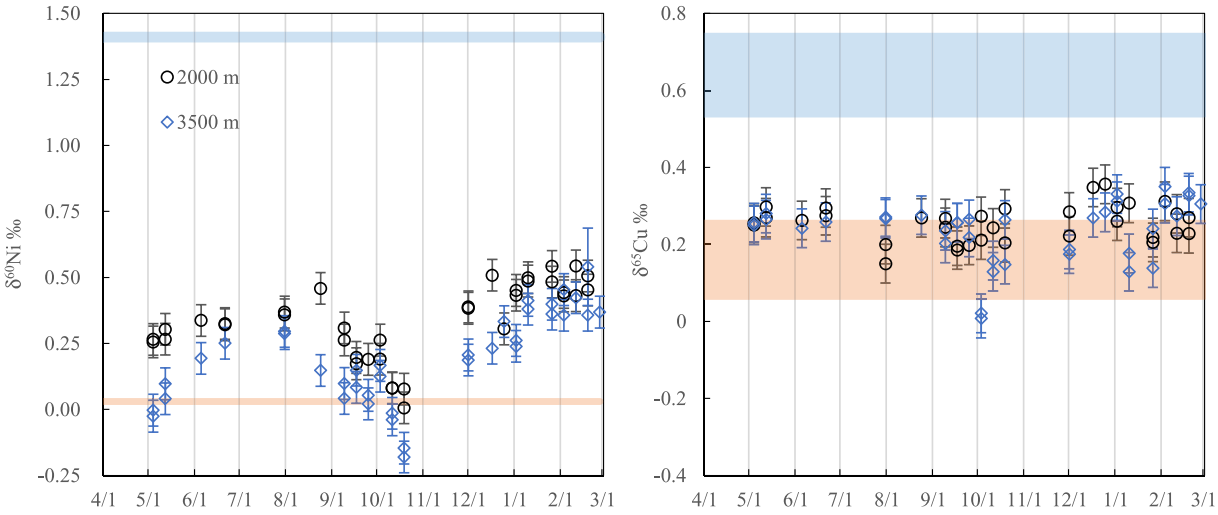

Fig. 4. Temporal variations in isotope ratios for Ni and Cu in sinking particles at depths of 2000 m (circles) and 3500 m (diamonds). The horizontal axis is the date from April 2014 to March 2015. Orange bands indicate the mean ± 1SD (one standard deviation) for δ^{60}Ni (0.03 ± 0.01‰; Gueguen et al., 2013) and δ^{65}Cu (0.16 ± 0.11‰; Little et al., 2017) in marine sediments. Blue bands indicate the mean ± 1SD for δ^{60}Ni (1.41 ± 0.04‰) and δ^{65}Cu (0.64 ± 0.10‰) in seawater at the South East Asian Time-series Study (SEATS) station. Error bars represent either 2SD of replicate analyses of BCR-414 or internal 2SE in multicollector inductively coupled plasma mass spectrometry (MC-ICPMS) measurement when this is the larger of the of the two errors. (For interpretation of the references to colour in this figure legend, the reader is referred to the web version of this article.)

2008).

The isotope ratios of Ni and Cu in sinking particles are shown in Fig. 4 and Table S4. In most cases, two divided subsamples are analyzed for each sinking particle sample. The duplicate analyses are in close agreement. The δ^{60}Ni values in sinking particles vary from +0.01‰ to +0.54‰ at a depth of 2000 m and −0.18‰ to +0.54‰ at a depth of 3500 m; temporal changes show a similar pattern between 2000 and 3500 m depth. In contrast, δ^{60}Ni values are slightly higher at a depth of 2000 m than at a depth of 3500 m; δ^{65}Cu values in sinking particles are relatively constant (+0.13‰ to +0.36‰) at both depths, with an exception in October at 3500 m.

4. Discussion

4.1. Sources of Ni and Cu in aerosols

Elevated aerosol Ni and Ti concentrations from January to April can be attributed to the influence of the northeastern monsoon carrying lithogenic and anthropogenic materials from East Asia to the NSCS. The ratios of Ni/Ti are 0.03 ± 0.02 mol/mol for PM 2.5–10 and 0.6 ± 0.3 mol/mol for PM 2.5 (mean ± 1SD, n = 38), which are 3 times and 60 times higher than the Ni/Ti ratio of 0.01 mol/mol in the upper continental crust, respectively (Chester and Jickells, 2012). Therefore, lithogenic aerosols are the minor source for Ni particularly in PM 2.5. Sea spray may be a possible source of Ni to explain the high Ni/Ti. Sodium is often used as a tracer of sea spray. Ni/Na ratios are 0.06 ± 0.03 mmol/mol for PM 2.5–10, and 2.0 ± 1.6 mmol/mol for PM 2.5, which is much higher than the Ni/Na ratio of ~0.02 μmol/mol in seawater. This means that Ni from sea spray is negligible in PM 2.5–10 and PM 2.5.

The Ni/Ti ratios in PM 2.5 are 1.0–3.4 mol/mol in Hong Kong (Ho et al., 2006) and 0.22 mol/mol in western Taiwan (Yunlin prefecture; Chen et al., 2015). Anthropogenic Ni is considered to be the dominant source in these regions. Similar Ni/Ti ratios are found in PM 2.5 collected in the NSCS. Therefore, PM 2.5 in the NSCS would contain much anthropogenic Ni from the surrounding cities. The Ni/Ti ratios in PM 2.5–10 are lower than those in PM 2.5. This can be explained by the contribution of lithogenic particles, as it is well known that wind-blown mineral dust is enriched in coarse particles with Ni/Ti of 0.01 mol/mol (Whitby, 1978). The concentrations of Ni in both PM 2.5 and PM 2.5–10 are strongly correlated with those of V (r = 0.92 for PM 2.5 and 0.87 for PM 2.5–10) over the sampling period (Table S5). These elements are known to be emitted to the atmosphere via crude oil combustion by ship traffic or power production (Jiang et al., 2014; Mueller et al., 2011; Okuda et al., 2007; Peltier and Lippmann, 2009; Tian et al., 2012). The Ni/V ratios are 0.56–0.57 mol/mol for PM 2.5 and 1.3–3.5 mol/mol for PM 2.5–10 collected in Hong Kong, an international port city, where Ni and V in aerosols are considered to be from crude oil combustion by ships (Jiang et al., 2014). In the NSCS, the Ni/V ratios are 0.45 ± 0.10 mol/mol for PM 2.5 (mean ± SD, n = 38) and 1.79 ± 1.33 mol/mol (n = 29) for PM 2.5–10. The Ni/V ratios of aerosols in the NSCS are similar to those in Hong Kong, suggesting that Ni from crude oil combustion is a major Ni source in the NSCS, also. The higher Ni/V ratios in PM 2.5–10 relative to PM 2.5 can be explained by a larger contribution of lithogenic aerosols with Ni/V ratios of ~2.4 mol/mol (from the composition in the upper continental crust; Chester and Jickells, 2012). The isotope ratios of Ni and the Ti/Ni ratios in PM 2.5 and PM 2.5–10 in the NSCS are compared with those in crude oil in Fig. 5 and Table S6. In Fig. 5, the data for PM 2.5 are plotted around the range of crude oil, excluding one sample (2011/5/9–15). For PM 2.5–10, the higher Ti/Ni ratios can be attributed to the elevated contribution of lithogenic particles, as mentioned earlier. Similar δ^{60}Ni values in crude oil and lithogenic particles cause undistinguishable δ^{60}Ni values between PM 2.5 and PM 2.5–10.

The ratios of Cu/Ti are 0.3 ± 0.4 mol/mol for PM 2.5–10 and 3 ± 4 mol/mol for PM 2.5, which are much higher than the Cu/Ti ratio of 0.006 mol/mol in the upper continental crust, respectively (Chester and Jickells, 2012). This indicates that the Cu originates from non-lithogenic sources. The Cu/Na ratios are 0.83 ± 1.7 mmol/mol for PM 2.5–10 and 9.7 ± 11 mmol/mol for PM 2.5, which are much higher than those of ~0.005 μmol/mol in seawater, suggesting a negligible contribution of Cu from sea spray. For PM 2.5 in coastal cities alongside the NSCS, the Cu/Ti ratio is 0.4–0.5 mol/mol in Yunlin (western Taiwan; Chen et al., 2015) and 3–7 mol/mol in Hong Kong (Ho et al., 2006). Since the PM 2.5 Cu/Ti ratio in the NSCS is at the level in Hong Kong, where Cu in PM 2.5 mainly originates from anthropogenic sources (Ho et al., 2006), anthropogenic Cu would be also dominant in the NSCS. Isotope ratios of Cu and Ti/Cu in PM 2.5 and PM 2.5–10 are compared with previously reported data for aerosols collected in London and Barcelona in Fig. 5 (Dong et al., 2017; Gonzalez

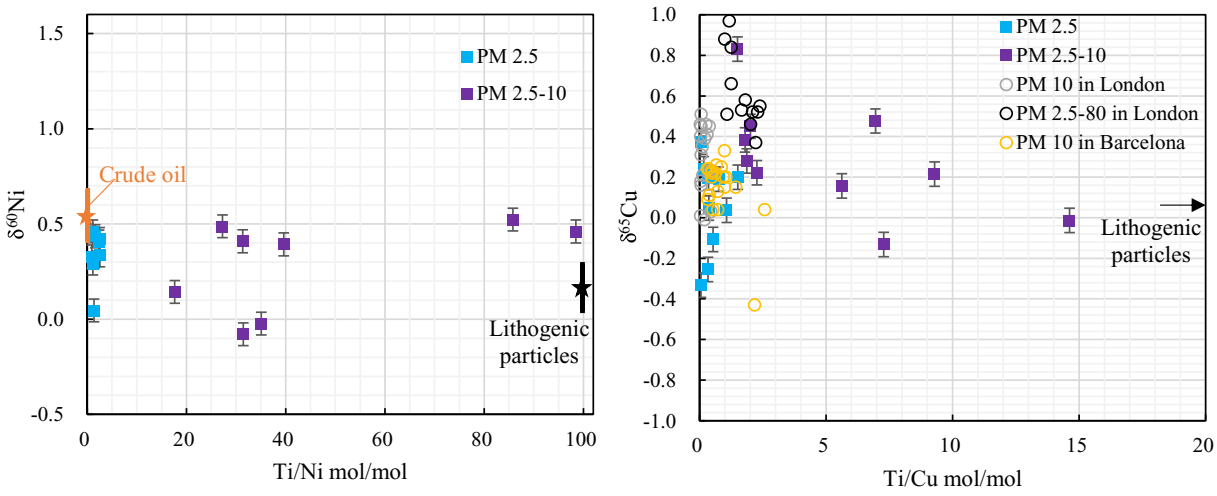

Fig. 5. Isotope ratios and elemental ratios for Ni and Cu in particulate matter (PM) 2.5 and PM 2.5–10. Light blue and purple squares indicate the data for PM 2.5 and PM 2.5–10, respectively. In the left panel, a black star indicates a mean value for lithogenic particles, and black bar indicates 1SD (one standard deviation) of the data. An orange star indicates a mean value for crude oil, and an orange bar indicates 1SD of the data. In the right panel, a mean value for lithogenic particles is located at the point (180, 0.01). Gray and black circles indicate the data for PM 10 and PM 2.5–80 in London, respectively (Dong et al., 2017; Gonzalez et al., 2016). Yellow circles indicate the data for PM 10 in Barcelona (Gonzalez et al., 2016). The data for lithogenic particles and crude oil, and their references, are summarized in Table S6. (For interpretation of the references to colour in this figure legend, the reader is referred to the web version of this article.)

et al., 2016). Our δ^{65}Cu values vary in a range similar to those observed in Barcelona (−0.4‰ to +0.3‰; Dong et al., 2017) and London (+0.0‰ to 1.0‰; Gonzalez et al., 2016, Dong et al., 2017). In those studies, high δ^{65}Cu values of +0.6‰ to +1.0‰ are attributed to the contribution of fuel oil combustion, and low δ^{65}Cu values of +0.0‰ to +0.6 are attributed to break wear emissions. Higher PM 2.5–10 Ti/Cu ratios in the NSCS as compared with London and Barcelona can be attributed to a higher contribution of lithogenic materials (Fig. 5). The concentrations of Cu in aerosols are substantially higher from May to September when an air mass comes from Southeast Asia or the North Pacific Ocean. This temporal change is different from that of the other metals (Fig. 2). Therefore, atmospheric Cu concentrations are not correlated with those of other metals (Table S5). As higher Cu concentrations are observed when an air mass comes from regions of low anthropogenic emission, we speculate that atmospheric Cu concentrations are affected by Cu emission from human activities in Dongsha Atoll. For example, blower motors in the air conditioners and vacuum pumps of the air samplers could be sources of Cu. Szymczak et al. (2007) have reported that particles emitted from electrical motors contain Cu at concentrations as high as 100–1000 times that of other heavy metals; this Cu is mainly distributed in the 0.3–10 μm particle range. Copper contamination from the exhaust of high-volume air samplers often derives from carbon brush wear in the vacuum pump (Landis et al., 2017; Patterson, 1980). Given that the possibility of Cu contamination cannot be ruled out, Cu concentrations and δ^{65}Cu values observed in aerosol samples at Dongsha Atoll may not be representative of those of the NSCS.

4.2. Sources of Ni and Cu in sinking particles

The fluxes for Ni, Cu, Ti, and P in sinking particles concordantly decrease from April 23 to October 24 and increase from 28 November. The similar temporal pattern of fluxes among the metals and biogenic matter is caused by processes associated with the winter monsoon. The winter monsoon carries lithogenic and anthropogenic materials to the oceanic region and also enhances vertical mixing of nutrients in the subsurface waters to the surface water, which may induce diatom bloom (Ran et al., 2015), and an increase in biogenic particles. Additionally, the winter monsoon produces eddies (Wang et al., 2012) that impact not only on surface water, but also on the bottom water on the shelf region. Zhang et al. (2014) observed an increase in suspended sediment concentrations near the bottom, off the coast of southwest Taiwan in the winter monsoon season, and suggested that these sediments are resuspended by eddies, and then transported to the NSCS. The higher Ti fluxes at 3500 m depth, as compared with 2000 m depth, in the NSCS are ascribed to this sediment transport from off southwest Taiwan (Fig. 3). Ho et al. (2011) observed similar results and suggested that the lithogenic particles are supplied from off southwest Taiwan. As with Ti, fluxes of Ni and Cu are higher at 3500 m depth than at 2000 m depth, which suggests that marine sediments off southwest Taiwan are one of the major sources of Ni and Cu in the sinking particles. However, for most of the sinking particles, the elemental ratios of Ni/Ti and Cu/Ti are higher than those of the marine sediments off southwest of Taiwan and have temporal variability, suggesting contributions from additional sources (Fig. 3).

To identify additional sources of Ni and Cu in sinking particles, isotope ratios (δ^{60}Ni and δ^{65}Cu) are plotted against elemental ratios of Ti, P, OC, and Mn to Ni and Cu (Fig. 6) together with those of potential sources. The isotopic and elemental ratios in potential sources are listed in Table S6. Ferromanganese oxides, which adsorb Ni, can be an additional source of Ni in sinking particles. However, δ^{60}Ni and Mn/Ni in the sinking particles are not on a mixing line between Fe−Mn oxides and marine sediments (Fig. 6g). Therefore, Fe−Mn oxides are not a significant source of Ni in sinking particles at the SEATS station. From Fig. 6a, the deposition of anthropogenic aerosols can be considered as an additional source of Ni in the sinking particles. We estimated the contribution of anthropogenic Ni in aerosols using Pb, which is well known as an anthropogenic tracer, as follows:

$$Ni_{anthropogenic} = \left(\frac{Ni}{Pb}\right)_{anthropogenic} \times Pb_{anthropogenic} \times \frac{(1 - sol_{Ni})}{(1 - sol_{Pb})} \quad (1)$$

$$Pb_{anthropogenic} = Pb_{total} - \left(\frac{Pb}{Ti}\right)_{lithogenic} \times Ti_{total} \quad (2)$$

where $Ni_{anthropogenic}$ and $Pb_{anthropogenic}$ are anthropogenic fluxes for Ni and Pb in sinking particles, respectively; and $(Ni/Pb)_{anthropogenic}$ is the ratio of Ni to Pb in bulk anthropogenic aerosols. The mean Ni/Pb ratio in PM 10 (the sum of PM 2.5 and PM 2.5–10) is 0.42 mol/mol at Dongsha Atoll. This value is used as $(Ni/Pb)_{anthropogenic}$. sol_{Ni} and sol_{Pb} are the solubility of Ni and Pb in PM 10, respectively. These parameters

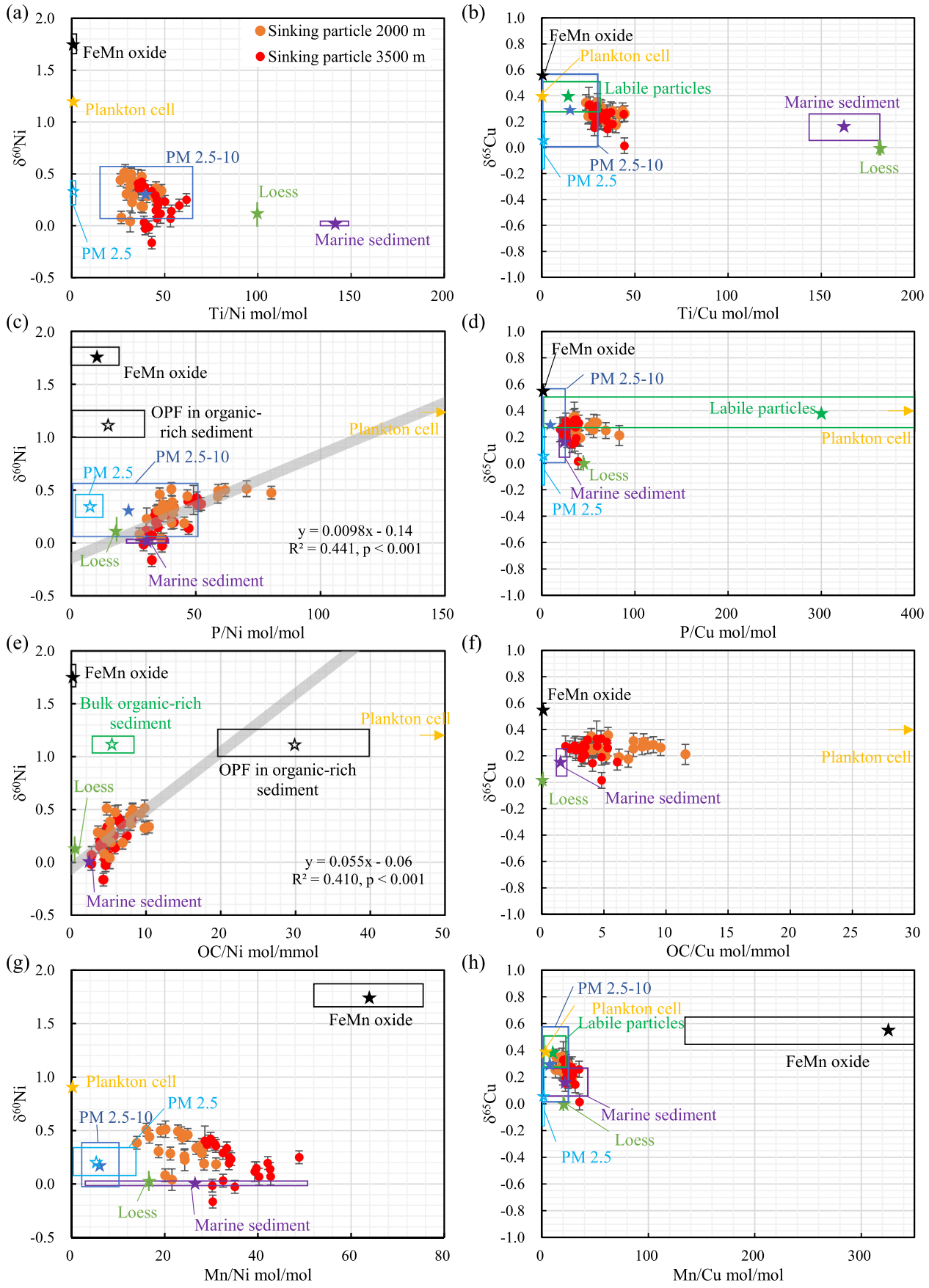

(caption on next page)

Fig. 6. Isotope ratios vs. elemental ratios of Ni or Cu. The δ^{60}Ni values are plotted against elemental ratios of Ni to Ti (a), P (c), OC (e), and Mn (g) in sinking particles. The δ^{65}Cu values are plotted against elemental ratios of Cu to Ti (b), P (d), OC (f), and Mn (h) in sinking particles. Orange and red circles indicate data for sinking particles at depths of 2000 and 3500 m, respectively. Stars indicate the mean values of data for potential sources of Ni and Cu in sinking particles. Boxes of the same colour with stars indicate 1SD (one standard deviation) of those data. The gray lines in panel (c) and (e) indicate the regression lines for the sinking particles. Mean values for plankton cells are located at (1400, 1.2) in panel (c), (2600, 0.4) in panel (d), (150, 1.2) in panel (e), and (280, 0.4) in panel (f). The data for potential sources and their references are summarized in Table S6. (For interpretation of the references to colour in this figure legend, the reader is referred to the web version of this article.)

were the same those in a previous study (Jiang et al., 2015). $Pb_{anthropogenic}$ is estimated using Eq. (2). The ratio of Pb/Ti in lithogenic materials, (Pb/Ti) lithogenic, is assumed to be 0.001 mol/mol, based on the composition of the upper continental crust (Chester and Jickells, 2012). Pb_{total} and Ti_{total} are fluxes of Pb and Ti for sinking particles, respectively. Estimated $Ni_{anthropogenic}$ accounts for only 7 ± 4% (mean ± SD) of the total flux of Ni for sinking particles at both depths. Therefore, anthropogenic aerosols have a small contribution to Ni in deep-sea sinking particles at the SEATS station.

In Fig. 6c and e, δ^{60}Ni is correlated with the P/Ni ratio ($y = 0.01\times - 0.14$, $r^2 = 0.44$, $p < .001$) and the OC/Ni ratio ($y = 0.06\times - 0.06$, $r^2 = 0.41$, $p < .001$). The regression lines pass near the plots for marine sediments off southwest Taiwan, implying that mixing of biogenic organic particles and marine sediments can account for the δ^{60}Ni. This is supported by previous studies for organic-rich marine sediments in upwelling regions off the coast of Peru. Böning et al. (2012, 2015) observed strong correlations between Ni and OC in various organic-rich marine sediments and suggested that Ni is brought from the water column to sediments by sinking with organic matter. Assuming that Ni in sinking particles is only from biogenic and lithogenic materials, mixing of these sources is represented by the following equation, as described by (Ho et al., 2011):

$$\frac{Ni}{Ti} = \left(\frac{Ni}{P}\right)_{biogenic} \times \left\{\frac{P}{Ti} - \left(\frac{P}{Ti}\right)_{lithogenic}\right\} + \left(\frac{Ni}{Ti}\right)_{lithogenic} \quad (3)$$

where Ni, Ti, and P indicate their fluxes; $(Ni/P)_{biogenic}$, $(Ni/Ti)_{lithogenic}$, and $(Ni/Ti)_{lithogenic}$ are constants of the Ni/P ratio in biogenic particles, and the P/Ti and Ni/Ti ratios in lithogenic particles, respectively. All Ti is assumed to be from lithogenic particles (Ti = 0 in biogenic particles). Based on Eq. (3), Ni/Ti ratios are plotted against P/Ti ratios for sinking particles at the SEATS station (Fig. 7). A linear correlation is found for sinking particles at each depth (2000 m, $r^2 = 0.43$, $p < .001$; 3500 m, $r^2 = 0.62$, $p < .001$), and for both depths ($r^2 = 0.54$, $p < .001$). Similarly, Ni/Ti ratios are plotted against OC/Ti ratios, and a significant correlation is found ($r^2 = 0.39$, $p < .001$). The correlations between Ni/Ti and P/Ti or OC/Ti are also found among various sedimentary samples, including deep-sea sinking particles from the Sargasso Sea (Conte et al., 2019; Huang and Conte, 2009; Jickells et al., 1984), marine sediments off southwest Taiwan (Chen and Kandasamy, 2008), and marine sediments in various upwelling regions (Böning et al., 2004; Brumsack, 2006; Ciscato et al., 2018). In Fig. S2, all of these data are plotted in the same way, showing similar trends to Fig. 7, although there are some outliers. The significant correlations between organic matter and Ni indicate that the enrichment of Ni in marine sediments and sinking particles is globally associated with biogenic organic matter.

The lithogenic materials in sinking particles at the SEATS station are mainly from resuspended marine sediments from off southwest Taiwan because these marine sediments show very low OC/Ti ratios (Chen and Kandasamy, 2008). Marine phytoplankton produce organic matter and take up trace metals into their cells as micronutrients. In the Pacific, intracellular Ni/P ratios in phytoplankton are reported to be 0.2–1.2 mmol/mol by single-cell analyses (Twining et al., 2011; Twining et al., 2014). For sinking particles at the SEATS station, ratios of Ni/OC and Ni/P in biogenic particles are estimated to be 0.09 and 8 mmol/mol, respectively. The estimated Ni/P ratio is 6.7–40 times higher than the intracellular Ni/P ratios. Twining et al. (2012) revealed that Ni in diatoms is equally distributed in soft tissue and silicate frustule. It was considered possible that Ni in biogenic particles at the SEATS station is dominantly contained in biogenic silica, since remineralization of silicate from biogenic silica is slower than that from organic matter (Boyd et al., 2017). However, the correlation between Ni/Ti and biogenic-Si/Ti ($r^2 = 0.24$, $n = 73$) in the sinking particles is weaker than that between Ni/Ti and P/Ti, indicating that biogenic silica is not the dominant source of Ni. The biogenic fraction of suspended particles has Ni/P ratios of 1.6 mmol/mol in the euphotic zone and ~5 mmol/mol in the oxygen minimum zone of the Eastern Tropical South Pacific (Ohnemus et al., 2017). The organic-pyrite fraction of organic-rich sediments off the coast of Peru have Ni/OC ratios of 0.04–0.08 mmol/mol, which is equivalent to Ni/P ratios of 4–8 mmol/mol assuming the Redfield C/P ratio (Ciscato et al., 2018). Ohnemus et al. (2017) attributed the high Ni/P ratios in the suspended particles to significant utilization of Ni by Ni-superoxide dismutase in marine organisms in the oxygen deficient zone. Ciscato et al. (2018) suggested that high Ni/P ratios in organic-rich sediments are ascribed to preferential remineralization of P and OC compared with Ni via respiration. We suggest another possibility, that dissolved Ni is adsorbed from seawater onto the organic matter of sinking particles. Balistrieri et al. (1981) suggested that organic matter controls the adsorption of dissolved metals onto marine particles. A recent study on modelling Zn cycles in the global ocean revealed that the sinking flux of Zn adsorbed from seawater onto organic matter of particles is much higher than that of intracellular Zn in the deep ocean (Weber et al., 2018). Since the complexation constants of Ni with organic compounds are similar to those of Zn (Balistrieri et al., 1981), Ni would be adsorbed onto the organic matter of particles along with Zn, and this can explain the high Ni/P ratios of the sinking particles. In the water column, concentrations of dissolved Ni correlate with those of dissolved P. Assuming that concentration gradients of dissolved Ni and P are produced by biological uptake and subsequent remineralization, the Ni/P ratio in phytoplankton is estimated from the slope of a regression line of dissolved Ni concentrations against dissolved P. This slope in the upper water column (< 800 m) is reported to be 1.0 to 1.8 mmol/mol in the North Pacific, the North Atlantic, and the Southern Ocean (Bruland, 1980; Sclater et al., 1976), which is similar to the intracellular Ni/P ratios estimated from the analyses of single cells of phytoplankton (0.2–1.2 mmol/mol; Twining et al., 2011, 2014), but lower than the Ni/P ratios in particulate organic matter estimated from the analyses of suspended particles in the oxygen minimum zone (~5 mmol/mol; Ohnemus et al., 2017), organic-rich marine sediments (4–8 mmol/mol; Ciscato et al., 2018), and sinking particles in this study (~8 mmol/mol). In addition, the linear relationship between dissolved concentrations of Ni and P is often broken in deep water (Bruland, 1980; Sclater et al., 1976), implying different behavior between particulate Ni and P in deep water. It is possible that the Ni/P ratio in biogenic organic particles would be modified in deep water via adsorption of Ni or preferential remineralization of P.

Although we are not able to identify the process of Ni enrichment in biogenic particles, δ^{60}Ni in the biogenic particles is estimated to be 1.1‰ based on the regression line for the P/Ni ratio (Fig. 6c) and 0.6‰ based on the regression line for the OC/Ni ratio (Fig. 6e). The former value is in a range of δ^{60}Ni in organic-pyrite fractions for surface organic-rich marine sediments (+0.9‰ to +1.3‰; Ciscato et al., 2018). δ^{60}Ni estimated for biogenic particles is lower than those in dissolved phase in seawater by 0.2–0.7‰, which suggests that biogenic particles

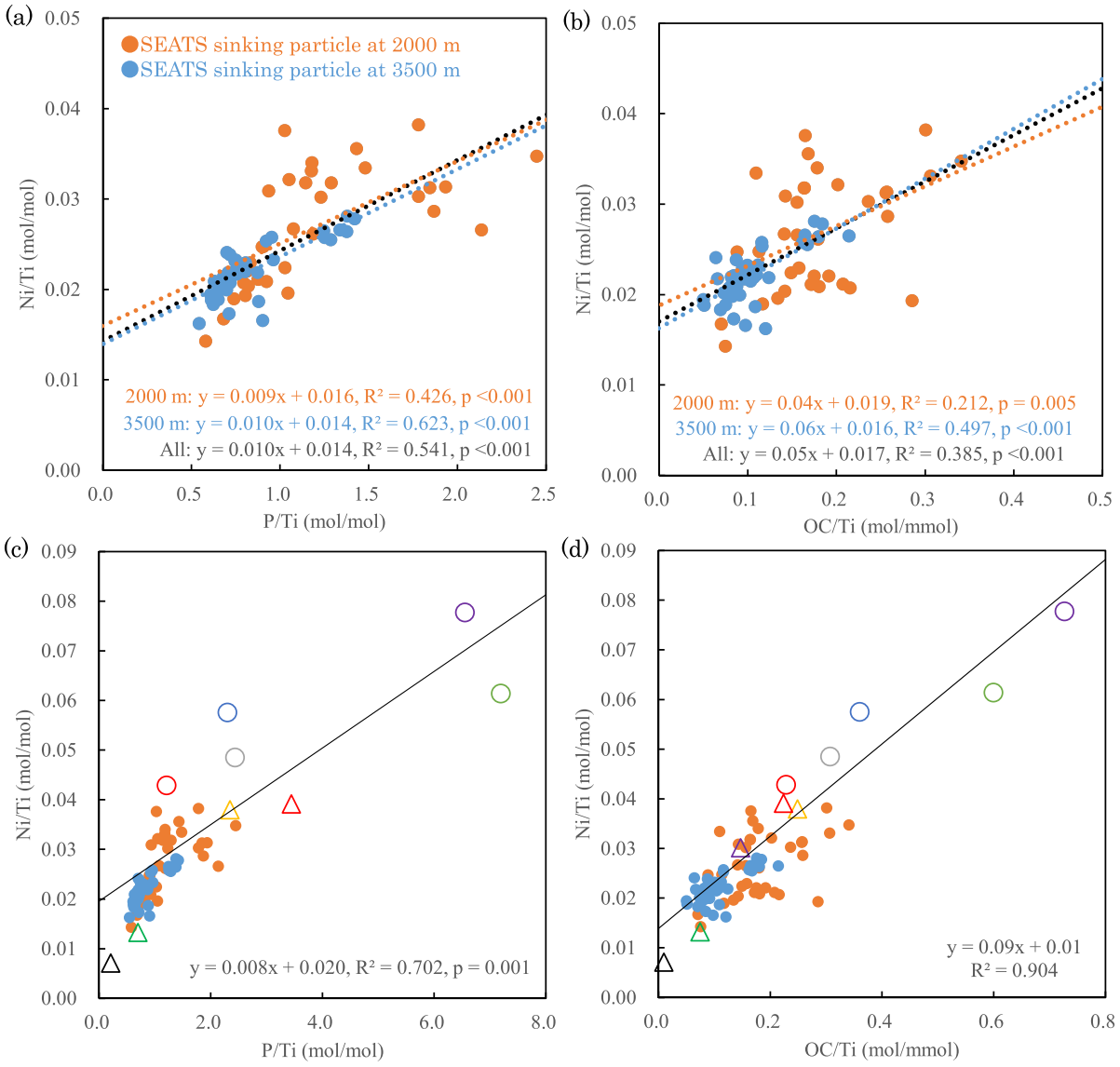

Average values: ○ sinking particle at 1500 m in the Sargasso Sea (Huang and Conte, 2009), ○ sinking particle at 3200 m in the Sargasso Sea (Huang and Conte, 2009), ○ sinking particle at 3200 m in the Sargasso Sea (Jickells et al., 1984), ○ sinking particle at 1500 m in the Sargasso Sea (Conte et al., 2018), ○ sinking particle at 3200 m in the Sargasso Sea (Conte et al., 2018), △ marine sediment off southwest Taiwan (Chen and Kandasamy, 2008), △ marine sediment off Peru (Böning et al., 2004), △ marine sediment off Peru (Ciscato et al., 2018), △ marine sediment off the Namibian coast (Brumsack, 2006), △ marine sediment in the Gulf of California (Brumsack, 2006)

Fig. 7. Plots of Ni/Ti vs. P/Ti or OC/Ti in sinking particles and modern marine sediments. Top panels show plots for the sinking particles at depths of 2000 m (orange closed circles) and 3500 m (blue closed circles) at the South East Asian Time-series Study (SEATS) station. Dotted lines indicate the regression lines for data at depths of 2000 m (orange), 3500 m (blue), and for both depths (black). Bottom panels show mean values of deep sinking particles from the Sargasso Sea (Ciscato et al., 2018; Conte et al., 2019; Huang and Conte, 2009; Jickells et al., 1984), and modern marine sediments in different oceanic regions (Böning et al., 2004; Brumsack, 2006; Chen and Kandasamy, 2008) overlaid on individual plots for sinking particles at the SEATS station. The solid line indicates the regression line for the mean values. (For interpretation of the references to colour in this figure legend, the reader is referred to the web version of this article.)

preferentially take up light isotopes of Ni from dissolved phase. The fractionation factor α defined as $(^{60}Ni/^{58}Ni)_{biogenic\ particle}/(^{60}Ni/^{58}Ni)_{seawater}$ is calculated to be 0.9993–0.9997. The biogenic particles have higher $\delta^{60}Ni$ and Ni/Ti than the lithogenic particles. Therefore, the decrease in $\delta^{60}Ni$ and Ni/Ti at 3500 m depth compared with 2000 m depth (Fig. 4) is due to a lower contribution of biogenic particles by remineralization and/or a larger input of resuspended marine sediments at a deeper layer.

Previous studies have reported isotopic imbalance between oceanic inputs and outputs of Ni (Cameron and Vance, 2014; Vance et al., 2016). The dominant oceanic input of Ni is river water, and the global mean of $\delta^{60}Ni$ for riverine input is +0.80‰ (Cameron and Vance, 2014). On the other hand, Fe–Mn oxides are considered as the dominant Ni sink in the ocean. The $\delta^{60}Ni$ in Fe–Mn crusts, as a proxy of authigenic Fe–Mn oxides, is in the range of +0.8‰ to +2.5‰ with the mean of +1.6‰ (Gall et al., 2013; Gueguen et al., 2016). To balance the oceanic budget for Ni isotopes, an isotopically light sink or heavy source is required. Biogenic particles are considered as a sink of dissolved Ni from seawater. Isotope ratios of Ni in biogenic particles are estimated to be +0.6‰ to +1.0‰, which is lighter than that of Fe–Mn crusts, and this sink reduces the imbalance of the oceanic budget for Ni isotopes.

We estimated the contribution of anthropogenic sources to Cu in sinking particles at the SEATS station using Eqs. (1) and (2). (Cu/

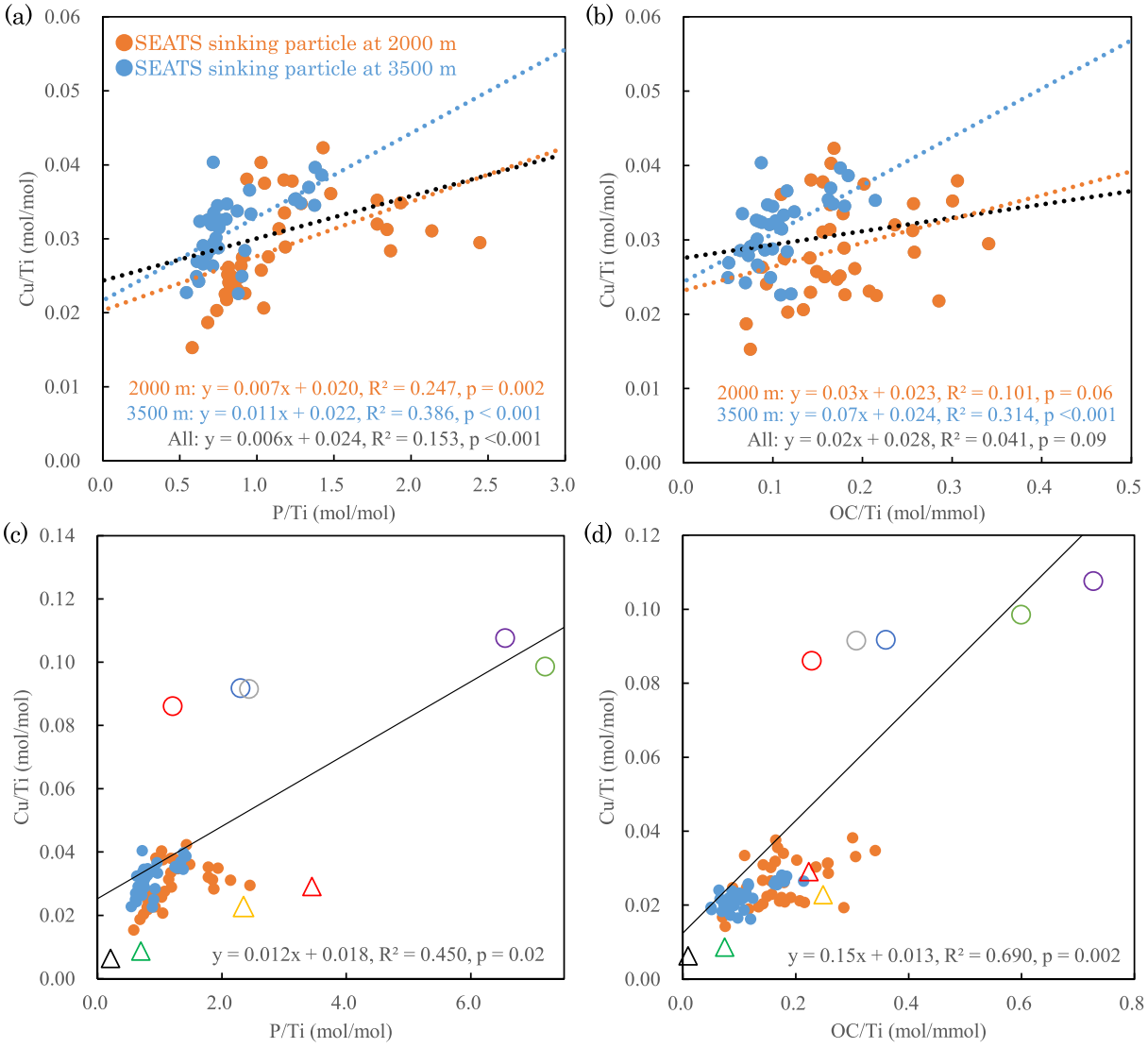

Average values: ○ sinking particle at 1500 m in the Sargasso Sea (Huang and Conte, 2009), ○ sinking particle at 3200 m in the Sargasso Sea (Huang and Conte, 2009), ○ sinking particle at 3200 m in the Sargasso Sea (Jickells et al., 1984), ○ sinking particle at 1500 m in the Sargasso Sea (Conte et al., 2018), ○ sinking particle at 3200 m in the Sargasso Sea (Conte et al., 2018), △ marine sediment off southwest Taiwan (Chen and Kandasamy, 2008), △ marine sediment off Peru (Böning et al., 2004), △ marine sediment off the Namibian coast (Brumsack, 2006), △ marine sediment in the Gulf of California (Brumsack, 2006)

Fig. 8. Plots of Cu/Ti vs. P/Ti or OC/Ti in sinking particles and modern marine sediments. Top panels show plots for sinking particles at depths of 2000 m (orange closed circles) and 3500 m (blue closed circles) at the South East Asian Time-series Study (SEATS) station. Dotted lines indicate the regression lines for data at depths of 2000 m (orange), 3500 m (blue), and at both depths (black). Bottom panels shows mean values of deep sinking particles from the Sargasso Sea (Conte et al., 2019; Huang and Conte, 2009; Jickells et al., 1984), and modern marine sediments in different oceanic regions (Böning et al., 2004; Brumsack, 2006; Chen and Kandasamy, 2008) overlaid on individual plots for sinking particles at the SEATS station. The solid line indicates the regression line for the mean values. (For interpretation of the references to colour in this figure legend, the reader is referred to the web version of this article.)

$Pb)_{anthropogenic}$ is assumed to be 2.9 mol/mol, which is the mean Cu/Pb ratio in PM 10 at Dongsha Atoll. Solubility of Cu and Pb in anthropogenic particles (sol_{Cu} and sol_{Pb}) are assumed to have the same values as a previous study (Jiang et al., 2015). The estimated anthropogenic flux of Cu accounts for 42 ± 23% (mean ± SD) of the total Cu flux for sinking particles. The percentage is higher than that for Ni. However, it should be noted that the Cu data from Dongsha Atoll may have been affected by local contamination (see Section 4.1). The Cu/P ratios in the sinking particles at the SEATS station are 20–60 mmol/mol, which are much higher than the intracellular Cu/P ratios of 0.07–1.36 mmol/mol from culture experiments (Ho, 2006) and 0.17–0.28 mmol/mol from a field study (Semeniuk et al., 2009; calculating from Cu/OC ratio with the Redfield C/P ratio of 106). Similar to Ni, suspended particles also have a Cu/P ratio that is higher than the intracellular ratio. In the Eastern Tropical South Pacific, the Cu/P ratio in biogenic fractions of suspended particles is 0.88 mmol/mol in the euphotic zone and 7.6 mmol/mol in the oxygen deficient zone (Ohnemus et al., 2017). In the South Atlantic, the Cu/P ratios in the labile fractions of marine particles are 0.5–11.5 mmol/mol in shallow water (40–400 m), and 30.9–89.1 mmol/mol in deep water (> 1000 m; Little et al., 2018). Little et al. (2018) suggested that Cu released via remineralization of particulate organic matter is re-adsorbed on residual sinking particles. The δ^{65}Cu values for sinking particles at the SEATS station are plotted against the ratio of Ti/Cu, P/Cu, and Mn/Cu (Fig. 6); all data plot between those for labile fractions of particles and marine sediments. The labile fractions of marine particles may be mainly associated with

organic matter. Therefore, major sources of Cu in the sinking particles are considered to be organic matter in addition to marine sediments off southwest Taiwan. The Cu/Ti ratio is plotted against the ratios of P/Ti and OC/Ti (Fig. 8). The correlations of Cu/Ti with P/Ti (r^2 = 0.15, p < .001) and with OC/Ti (r^2 = 0.04, p = .09; Fig. 8) are weaker than those for Ni. This may be ascribed to variable Cu concentrations in organic matter depending on the effects of scavenging through the water column. Large variations in the P/Cu ratio in labile fractions of particles in the South Atlantic support this possibility (Little et al., 2018). Otherwise, additional Cu sources, such as Fe−Mn oxides and anthropogenic aerosols, may perturb the correlations of Cu with P or OC. Fairly constant δ^{65}Cu values in sinking particles at the SEATS station are due to similar δ^{65}Cu values between Cu adsorbed on organic particles (~0.4‰; Little et al., 2018) and Cu from marine sediments (~0.2‰; Little et al., 2017).

5. Conclusions

Sinking particles, aerosols, and seawater collected in the NSCS were studied to understand the marine geochemistry of stable isotopes of Ni and Cu. In aerosols, δ^{60}Ni and δ^{65}Cu values are different from those of lithogenic materials, indicating that the aerosols are dominated by anthropogenic sources. In sinking particles, the linear relationships between δ^{60}Ni and P/Ni or OC/Ti in the sinking particles suggest that the main sources of Ni are marine sediments resuspended off the southwest coast of Taiwan, and biogenic organic particles. In the biogenic organic particles, the Ni/P and Ni/OC ratios are estimated to be 8 and 0.09 mmol/mol, respectively. These ratios are much higher than the intracellular ratios revealed by single-cell analyses of phytoplankton as reported by Twining and Baines (2013), but similar to those of suspended particles in the oxygen minimum zone of the Eastern Tropical South Pacific (Ohnemus et al., 2017), and those of organic-rich sediments off the coast of Peru (Ciscato et al., 2018). High Ni/P and Ni/OC ratios in biogenic organic particles are possibly caused by preferential remineralization of P and OC compared with Ni or adsorption of dissolved Ni onto the organic matter of particles. The δ^{60}Ni in the biogenic organic particles is estimated to be +0.6‰ to +1.0‰, indicating that biogenic particles contain light Ni isotopes by +0.3‰ to +0.7‰, compared with dissolved δ^{60}Ni in seawater. Copper isotope ratios in the sinking particles are relatively constant (+0.13‰ to +0.36‰) and are between those for marine sediments (0.4%; Little et al., 2017) and labile fractions of marine particles (0.2%; Little et al., 2018). The sources of Cu in the sinking particles are likely to be marine sediments and organic matter. The correlations between Cu and P or OC are weaker than that of Ni. This suggests that the Cu/P and Cu/OC ratios are not constant in organic matter or there are additional sources of particulate Cu, such as Fe−Mn oxides and anthropogenic aerosols.

Acknowledgements

We would like to thank Wan-Yen Cheng, Wan-Chen Tu, Chih-Chiang Hsieh, Hung-Yu Chen, and the staff of the Taiwan Ocean Research Institute, for providing technical and sampling support. Data for sinking particles in the Sargasso Sea are from the Oceanic Flux Program time-series. This work was supported by the International Short-term Exchange Program for Young Researchers and the International Collaborative Research Program (2017-89 and 2019-47) from the Institute for Chemical Research, Kyoto University. This work was also supported by the Joint Research Grant for Environmental Isotope Study from the Research Institute for Humanity and Nature, and JSPS KAKENHI Grants (JP18033453 and JP19095237).

Appendix A. Supplementary data

Supplementary data to this article can be found online at https://doi.org/10.1016/j.marchem.2020.103751.

References

Baconnais, I., Rouxel, O., Dulaquais, G., Boye, M., 2019. Determination of the copper isotope composition of seawater revisited: A case study from the Mediterranean Sea. Chem. Geol. 511, 465–480.
Balistrieri, L., Brewer, P.G., Murray, J.W., 1981. Scavenging residence times of trace metals and surface chemistry of sinking particles in the deep ocean. Deep Sea Res. A Oceanogr. Res. Papers 28 (2), 101–121.
Barwise, A.J.G., 1990. Role of nickel and vanadium in petroleum classification. Energy Fuel 4 (6), 647–652.
Böning, P., et al., 2004. Geochemistry of Peruvian near-surface sediments. Geochim. Cosmochim. Acta 68 (21), 4429–4451.
Böning, P., Fröllje, H., Beck, M., Schnetger, B., Brumsack, H.J., 2012. Underestimation of the authigenic fraction of Cu and Ni in organic-rich sediments. Mar. Geol. 323–325, 24–28.
Böning, P., Shaw, T., Pahnke, K., Brumsack, H.-J., 2015. Nickel as indicator of fresh organic matter in upwelling sediments. Geochim. Cosmochim. Acta 162, 99–108.
Boyd, P.W., Ellwood, M.J., Tagliabue, A., Twining, B.S., 2017. Biotic and abiotic retention, recycling and remineralization of metals in the ocean. Nat. Geosci. 10, 167.
Boyle, E.A., Sclater, F.R., Edmond, J.M., 1977. The distribution of dissolved copper in the Pacific. Earth Planet. Sci. Lett. 37 (1), 38–54.
Boyle, E.A., Huested, S.S., Jones, S.P., 1981. On the distribution of copper, nickel, and cadmium in the surface waters of the North Atlantic and North Pacific Ocean. J. Geophys. Res. Oceans 86 (C9), 8048–8066.
Bruland, K.W., 1980. Oceanographic distributions of cadmium, zinc, nickel, and copper in the North Pacific. Earth Planet. Sci. Lett. 47 (2), 176–198.
Brumsack, H.-J., 2006. The trace metal content of recent organic carbon-rich sediments: implications for Cretaceous black shale formation. Palaeogeogr. Palaeoclimatol. Palaeoecol. 232 (2), 344–361.
Cameron, V., Vance, D., 2014. Heavy nickel isotope compositions in rivers and the oceans. Geochim. Cosmochim. Acta 128 (0), 195–211.
Chen, C.-T., Kandasamy, S., 2008. Evaluation of elemental enrichments in surface sediments off southwestern Taiwan. Environ. Geol. 54 (6), 1333–1346.
Chen, Y.-C., et al., 2015. Characteristics of concentrations and metal compositions for PM2.5 and PM2.5–10 in Yunlin County, Taiwan during air quality deterioration. Aerosol Air Qual. Res. 15 (7), 2571–2583.
Chester, R., Jickells, T., 2012. Marine Geochemistry. Willey-Blackwell, Hoboken, N.J.
Ciscato, E.R., Bontognali, T.R.R., Vance, D., 2018. Nickel and its isotopes in organic-rich sediments: implications for oceanic budgets and a potential record of ancient seawater. Earth Planet. Sci. Lett. 494, 239–250.
Conte, M.H., Carter, A.M., Koweek, D.A., Huang, S., Weber, J.C., 2019. The elemental composition of the deep particle flux in the Sargasso Sea. Chem. Geol. 511, 279–313.
Dong, S., et al., 2017. Isotopic signatures suggest important contributions from recycled gasoline, road dust and non-exhaust traffic sources for copper, zinc and lead in PM10 in London, United Kingdom. Atmos. Environ. 165, 88–98.
Duce, R.A., et al., 1991. The atmospheric input of trace species to the world ocean. Glob. Biogeochem. Cycles 5 (3), 193–259.
Elliott, T., Steele, R.C.J., 2017. The isotope geochemistry of Ni. Rev. Mineral. Geochem. 82 (1), 511–542.
Gall, L., et al., 2013. Nickel isotopic compositions of ferromanganese crusts and the constancy of deep ocean inputs and continental weathering effects over the Cenozoic. Earth Planet. Sci. Lett. 375, 148–155.
Gonzalez, R.O., et al., 2016. New insights from zinc and copper isotopic compositions into the sources of atmospheric particulate matter from two major European cities. Environ. Sci. Technol. 50 (18), 9816–9824.
Gueguen, B., Rouxel, O., Ponzevera, E., Bekker, A., Fouquet, Y., 2013. Nickel isotope variations in terrestrial silicate rocks and geological reference materials measured by MC-ICP-MS. Geostand. Geoanal. Res. 37 (3), 297–317.
Gueguen, B., et al., 2016. Comparative geochemistry of four ferromanganese crusts from the Pacific Ocean and significance for the use of Ni isotopes as paleoceanographic tracers. Geochim. Cosmochim. Acta 189, 214–235.
Ho, T.-Y., 2006. The trace metal composition of marine microalgae in cultures and natural assemblages. In: Rao, D.V.S. (Ed.), Algal Cultures: Analogues of Blooms and Applications. Science Publishers, pp. 271–299.
Ho, K.F., Cao, J.J., Lee, S.C., Chan, C.K., 2006. Source apportionment of PM2.5 in urban area of Hong Kong. J. Hazard. Mater. 138 (1), 73–85.
Ho, T.-Y., Wen, L.-S., You, C.-F., Lee, D.-C., 2007. The trace metal composition of size-fractionated plankton in the South China Sea: biotic versus abiotic sources. Limnol. Oceanogr. 52 (5), 1776–1788.
Ho, T.-Y., et al., 2010. Trace metal cycling in the surface water of the South China Sea: vertical fluxes, composition, and sources. Limnol. Oceanogr. 55 (5), 1807–1820.
Ho, T.-Y., Chou, W.-C., Lin, H.-L., Sheu, D.D., 2011. Trace metal cycling in the deep water of the South China Sea: the composition, sources, and fluxes of sinking particles. Limnol. Oceanogr. 56 (4), 1225–1243.
Huang, S., Conte, M.H., 2009. Source/process apportionment of major and trace elements in sinking particles in the Sargasso Sea. Geochim. Cosmochim. Acta 73 (1), 65–90.
Hulskotte, J.H.J., Denier van der Gon, H.A.C., Visschedijk, A.J.H., Schaap, M., 2007. Brake wear from vehicles as an important source of diffuse copper pollution. Water Sci. Technol. 56 (1), 223–231.
Jiang, S.Y.N., Yang, F., Chan, K.L., Ning, Z., 2014. Water solubility of metals in coarse PM and PM2.5 in typical urban environment in Hong Kong. Atmos. Pollut. Res. 5 (2), 236–244.
Jiang, S.Y., Kaul, D.S., Yang, F., Sun, L., Ning, Z., 2015. Source apportionment and water solubility of metals in size segregated particles in urban environments. Sci. Total Environ. 533, 347–355.

Jickells, T.D., Deuser, W.G., Knap, A.H., 1984. The sedimentation rates of trace elements in the Sargasso Sea measured by sediment trap. Deep Sea Res. A Oceanogr. Res. Papers 31 (10), 1169–1178.
John, S.G., Conway, T.M., 2014. A role for scavenging in the marine biogeochemical cycling of zinc and zinc isotopes. Earth Planet. Sci. Lett. 394, 159–167.
Landis, M.S., et al., 2017. Source apportionment of ambient fine and coarse particulate matter at the Fort McKay community site, in the Athabasca Oil Sands Region, Alberta, Canada. Sci. Total Environ. 584–585, 105–117.
Liao, W.-H., Yang, S.-C., Ho, T.-Y., 2017. Trace metal composition of size-fractionated plankton in the Western Philippine Sea: the impact of anthropogenic aerosol deposition. Limnol. Oceanogr. 62 (5), 2243–2259.
Little, S.H., Vance, D., Walker-Brown, C., Landing, W.M., 2014. The oceanic mass balance of copper and zinc isotopes, investigated by analysis of their inputs, and outputs to ferromanganese oxide sediments. Geochim. Cosmochim. Acta 125 (0), 673–693.
Little, S.H., Vance, D., McManus, J., Severmann, S., Lyons, T.W., 2017. Copper isotope signatures in modern marine sediments. Geochim. Cosmochim. Acta 212, 253–273.
Little, S.H., Archer, C., Milne, A., Schlosser, C., Achterberg, E.P., Lohan, M.C., Vance, D., 2018. Paired dissolved and particulate phase Cu isotope distributions in the South Atlantic. Chem. Geol. 502, 29–43.
Maréchal, C.N., Nicolas, E., Douchet, C., Albarède, F., 2000. Abundance of zinc isotopes as a marine biogeochemical tracer. Geochem. Geophys. Geosyst. 1 (5) n/a-n/a.
Morel, F.M.M., Price, N.M., 2003. The biogeochemical cycles of trace metals in the oceans. Science 300 (5621), 944–947.
Moynier, F., Vance, D., Fujii, T., Savage, P., 2017. The isotope geochemistry of zinc and copper. Rev. Mineral. Geochem. 82 (1), 543–600.
Mueller, D., Uibel, S., Takemura, M., Klingelhoefer, D., Groneberg, D.A., 2011. Ships, ports and particulate air pollution - an analysis of recent studies. J. Occup. Med. Toxicol. 6 (1), 31.
Ohnemus, D.C., Lam, P.J., 2015. Cycling of lithogenic marine particles in the US GEOTRACES North Atlantic transect. Deep-Sea Res. II Top. Stud. Oceanogr. 116, 283–302.
Ohnemus, D.C., et al., 2017. Elevated trace metal content of prokaryotic communities associated with marine oxygen deficient zones. Limnol. Oceanogr. 62 (1), 3–25.
Okuda, T., Nakao, S., Katsuno, M., Tanaka, S., 2007. Source identification of nickel in TSP and PM2.5 in Tokyo, Japan. Atmos. Environ. 41 (35), 7642–7648.
Pacyna, J.M., Pacyna, E.G., 2001. An assessment of global and regional emissions of trace metals to the atmosphere from anthropogenic sources worldwide. Environ. Rev. 9 (4), 269–298.
Patterson, R.K., 1980. Aerosol contamination from high-volume sampler exhaust. J. Air Pollut. Control Assoc. 30 (2), 169–171.
Peltier, R.E., Lippmann, M., 2009. Residual oil combustion: 2. Distributions of airborne nickel and vanadium within New York City. J. Expos. Sci. Environ. Epidemiol. 20, 342.
Ran, L., et al., 2015. Variability in the abundance and species composition of diatoms in sinking particles in the northern South China Sea: results from time-series moored sediment traps. Deep-Sea Res. II Top. Stud. Oceanogr. 122, 15–24.
Sclater, F.R., Boyle, E., Edmond, J.M., 1976. On the marine geochemistry of nickel. Earth Planet. Sci. Lett. 31 (1), 119–128.
Semeniuk, D.M., et al., 2009. Plankton copper requirements and uptake in the subarctic Northeast Pacific Ocean. Deep-Sea Res. I Oceanogr. Res. Papers 56 (7), 1130–1142.
Sherrell, R.M., Boyle, E.A., 1992. The trace metal composition of suspended particles in the oceanic water column near Bermuda. Earth Planet. Sci. Lett. 111 (1), 155–174.
Souto-Oliveira, C.E., Babinski, M., Araújo, D.F., Andrade, M.F., 2018. Multi-isotopic fingerprints (Pb, Zn, Cu) applied for urban aerosol source apportionment and discrimination. Sci. Total Environ. 626, 1350–1366.
Souto-Oliveira, C.E., Babinski, M., Araújo, D.F., Weiss, D.J., Ruiz, I.R., 2019. Multi-isotope approach of Pb, Cu and Zn in urban aerosols and anthropogenic sources improves tracing of the atmospheric pollutant sources in megacities. Atmos. Environ. 198, 427–437.
Suvarapu, L.N., Baek, S.-O., 2017. Determination of heavy metals in the ambient atmosphere: a review. Toxicol. Ind. Health 33 (1), 79–96.
Szymczak, W., Menzel, N., Keck, L., 2007. Emission of ultrafine copper particles by universal motors controlled by phase angle modulation. J. Aerosol Sci. 38 (5), 520–531.
Takano, S., Tanimizu, M., Hirata, T., Sohrin, Y., 2014. Isotopic constraints on biogeochemical cycling of copper in the ocean. Nat. Commun. 5.
Takano, S., et al., 2017. A simple and rapid method for isotopic analysis of nickel, copper, and zinc in seawater using chelating extraction and anion exchange. Anal. Chim. Acta 967, 1–11.
Teng, F.-Z., Dauphas, N., Watkins, J.M., 2017. Non-traditional stable isotopes: retrospective and prospective. Rev. Mineral. Geochem. 82 (1), 1–26.
Thompson, C.M., Ellwood, M.J., 2014. Dissolved copper isotope biogeochemistry in the Tasman Sea, SW Pacific Ocean. Mar. Chem. 165 (0), 1–9.
Tian, H.Z., et al., 2012. Anthropogenic atmospheric nickel emissions and its distribution characteristics in China. Sci. Total Environ. 417–418, 148–157.
Twining, B.S., Baines, S.B., 2013. The trace metal composition of marine phytoplankton. Annu. Rev. Mar. Sci. 5 (1), 191–215.
Twining, B.S., et al., 2011. Metal quotas of plankton in the equatorial Pacific Ocean. Deep-Sea Res. II Top. Stud. Oceanogr. 58 (3), 325–341.
Twining, B.S., Baines, S.B., Vogt, S., Nelson, D.M., 2012. Role of diatoms in nickel biogeochemistry in the ocean. Glob. Biogeochem. Cycles 26 (4) n/a-n/a.
Twining, B.S., et al., 2014. Differential remineralization of major and trace elements in sinking diatoms. Limnol. Oceanogr. 59 (3), 689–704.
Vance, D., et al., 2008. The copper isotope geochemistry of rivers and the oceans. Earth Planet. Sci. Lett. 274 (1–2), 204–213.
Vance, D., et al., 2016. The oceanic budgets of nickel and zinc isotopes: the importance of sulfidic environments as illustrated by the Black Sea. Philos. Trans. R. Soc. A Math. Phys. Eng. Sci. 374 (2081).
Ventura, G.T., et al., 2015. The stable isotope composition of vanadium, nickel, and molybdenum in crude oils. Appl. Geochem. 59, 104–117.
Wang, G., Li, J., Wang, C., Yan, Y., 2012. Interactions among the winter monsoon, ocean eddy and ocean thermal front in the South China Sea. J. Geophys. Res. Oceans 117 (C8).
Wang, R.M., Archer, C., Bowie, A.R., Vance, D., 2019. Zinc and nickel isotopes in seawater from the Indian Sector of the Southern Ocean: the impact of natural iron fertilization versus Southern Ocean hydrography and biogeochemistry. Chem. Geol. 511, 452–464.
Weber, T., John, S., Tagliabue, A., DeVries, T., 2018. Biological uptake and reversible scavenging of zinc in the global ocean. Science 361 (6397), 72–76.
Wen, L.-S., Jiann, K.-T., Santschi, P.H., 2006. Physicochemical speciation of bioactive trace metals (Cd, Cu, Fe, Ni) in the oligotrophic South China Sea. Mar. Chem. 101 (1), 104–129.
Whitby, K.T., 1978. The physical characteristics of sulfur aerosols. Atmos. Environ. (1967) 12 (1), 135–159.
Yang, S.-C., Lee, D.-C., Ho, T.-Y., 2012. The isotopic composition of Cadmium in the water column of the South China Sea. Geochim. Cosmochim. Acta 98, 66–77.
Zhang, Y., et al., 2014. Mesoscale eddies transport deep-sea sediments. Sci. Rep. 4, 5937.